Load transfer within the bolted joint of a laminate made from ultra-high molecular weight polyethylene fibres

S. P. H. Skovsgaard[a,b], H. M. Jensen[b] and N. A. Fleck[a]*

[a] Department of Engineering, University of Cambridge, Trumpington Street, Cambridge, UK

[b] Department of Engineering, Aarhus University, Inge Lehmanns Gade 10, Aarhus C, Denmark

*Corresponding author

26 April 2019

Submitted to the International Journal of Solids and Structures

Abstract

The mechanism of load transfer within the bolted joint of a laminate sheet made from ultra-high molecular weight polyethylene (UHMWPE) plies is investigated both experimentally and by an analytical model. The nature of load transfer and the active failure mechanisms are obtained as a function of joint geometry and of the lateral clamping force on the faces of the laminate (by pre-tensioning of the bolt). A combination of X-ray tomography and optical microscopy reveal that the dominant failure mechanism in the clamped joint is shear failure involving splits of the 0º plies and sliding at the interface between the 0° and 90° plies. A simple analytical model is developed for this shear failure mechanism and, upon noting the competing failure mechanisms of bearing failure, bolt shear and of tensile failure of the 0° plies, a failure mechanism map is constructed in terms of the geometry of the bolted joint, for the case of no pre-tension of the bolt. The analytical model for shear failure suggests that the enhancement in joint strength with increased pre-tensioning of bolt is due to the fact that the shear strength of the UHMWPE increases with increasing hydrostatic pressure.

Keywords: UHMWPE fibres; Joint failure; Failure map; Pressure dependent shear strength

1. Introduction

Ultra-high molecular weight polyethylene (UHMWPE) fibres embedded in a polyurethane matrix have a high specific modulus and a high specific strength, and are commonly used for personnel and vehicle armour. Additionally, UHMWPE fibres are used for ropes, nets, footwear, cut resistant gloves and for air cargo containers. The company DSM[1] commercialized fibres made from UHMWPE in the late 1970s under the trade name Dyneema®. UHMWPE has extremely long molecular chains and, when fibres are produced using a gel-spinning/hot drawing process, the fibres possess a high strength on the order of 3 GPa, Russell et al. (2013). The fibres are coated in a polyurethane (PU) resin solution and are then formed into [0/90/0/90] stacks. The PU solvent is removed during a drying process and the stacks are then hot pressed.

Several studies have been performed to determine the mechanical properties of UHMWPE fibres and composite plates. In the early work of Wilding and Ward (1978), the creep and recovery of ultra-high modulus polyethylene fibres were determined. Smith and Lemstra (1980) conducted one of the early studies that lead to the choice of fibres used in Dyneema®. They measured the effect of draw ratio upon the tensile modulus and strength, and concluded that an extension ratio of $\lambda = 32$ by hot drawing led to a fibre strength of 3.0 GPa and a Young’s modulus of 90 GPa. More recently, Govaert and Lemstra (1992) and Govaert and Peijs (1995) explored the sensitivity of the tensile response of UHMWPE fibres to temperature and to strain-rate.

Over the past decade, several authors have developed models to predict the ballistic performance of UHMWPE composite plates; for example, Grujicic et al. (2009) have developed a continuum-damage based constitutive model and implemented it within a finite element (FE)

[1] DSM, Het Overloon 1, 6411 TE Heerlen, The Netherlands.

code. Iannucci and Pope (2011) have developed a model for the impact response of sheets made from high performance polymer fibres. Koh et al. (2010) investigated the behaviour of UHMWPE yarns by both quasi-static and dynamic tests. Additionally, Karthikeyan et al. (2013) performed quasi-static and dynamic impact tests on composite plates made from either UHMWPE fibres or carbon fibre-reinforced polymers. They observed that composites of high indentation strength in the quasi-static tests also had a high failure impulse. Russell et al. (2013) created a series of test methods for the mechanical performance of fibres, yarns and laminates made from UHMWPE. They highlighted the need to develop new geometries for tensile testing due to the difficulties in transferring load into laminates made from UHMWPE. A practical means of exploring load transfer in the presence of confinement is to transfer load via bolted joints: this motivates the current study.

We emphasise that it is difficult to measure the mechanical properties of laminates made from UHMWPE using conventional test methods due to the very low shear strength of both fibres and matrix. Consequently, indirect test methods have been developed. For example, Attwood et al. (2014) developed an out-of-plane compression test to determine the pressure sensitivity of UHWMPE laminates. The inter-layer strength was measured by Liu et al. (2014) via tests on an end-loaded cantilever beam. They extracted the elastic and plastic properties by varying the load level and by suitable positioning of the loading pin; a FE-model was used to aid interpretation of their results. The compressive response of UHWMPE fibres, and composite plates made from UHMWPE, was determined experimentally by Attwood et al. (2015) and was compared with fibre-kinking theory. In a recent study, Liu et al. (2018) determined the Mode I and II fracture toughness of a UHMWPE laminate. They performed a penetration experiment with a sharp-tipped punch and compared the measurements with a FE-model based upon a crystal plasticity model for the ply behaviour. Karthikeyan et al. (2013) performed both quasi-static loading and dynamic impact tests on end-clamped UHMWPE beams. They found that the method of confinement had a large influence on both the quasi-static and dynamic behaviours.

Several investigations have been performed on the mechanics of mechanically fastened joints in fibre-reinforced polymers. A failure mechanism map for single-lap bolted joints in CFRP laminates was constructed by Smith et al. (1986) on the basis of a set of tests on multidirectional CFRP laminates. Failure was by net-section tension, bearing or by shear-out along splits within the 0º plies. A similar methodology is followed in the present study. Camanho and Matthews (1997) distinguished five failure modes of composite joints: tension, shear, cleavage, bearing and a pull-through failure mode. A decade later, Thoppul et al. (2009) made a thorough review of the state-of-the-art methods to study the failure of composite joints. The focus in these previous studies was on glass and carbon fibre-reinforced polymers. In the present study, we shall explore the extent to which these failure mechanisms persist in UHMWPE laminates of high in-plane strength but of very low shear strength.

2. Test method

We investigated the mechanism of load transfer into a bolted joint comprising HB26 Dyneema® [0°/90°] plates with and without transverse clamping. The plates had equal volume fractions of 0° and 90° plies and a ply thickness of h = 60 μm. Specimens of overall thickness t = 6.5 mm and ply layup $(0°, 90°)_{54}$ were machined to the geometry as depicted in Fig. 1(a), with bolt diameter d = 8 mm, ligament width w = 6 mm and ligament height b = 2, 4, 6 or 8 mm. The lower part of each specimen was clamped between two hardened steel plates using eleven M4 (Grade 12.9[2]) steel bolts. The need for a large number of small bolts to introduce load into the specimen without local joint failure at each of the small bolts is traced to the fact that UHMWPE laminates have a high tensile strength but a low shear strength. Special measures must be taken to ensure load introduction into the specimen, as discussed by Russell et al. (2013). The variables b and w for the ligament dimensions are used in the present study in order

[2] ASTM F568M

to emphasise their role. They are closely related to the overall width of the joint $W = 2w + d$ and to the end-distance from the centre of the bolt to the free edge of the plate $e = b + d/2$.

An in-plane bearing load F was imposed on each specimen via a steel bolt (Grade[2] 12.9) of diameter d and thick washers (that is, clamping rings) of diameter d_w = 25 mm; this was achieved by the loading arrangement of Fig. 1(b). In addition, the effect of the clamping pre-load T_0 in the bolt upon the shear response was investigated by suitable torqueing of the bolt. The bolt was displaced in the x_1 direction relative to the composite panel using a screw-driven test machine with a displacement rate of 1 mm/min. The bolt displacement u was measured by a laser extensometer and the reaction force F was determined by the load cell of the test machine. The transverse clamping force T was measured via an in-house load cell consisting of two 120 Ω strain gauges mounted on the opposing walls of an aluminium alloy tube. The strain gauges were of dimension 3 mm x 1 mm and of gauge factor 2.15, and a Wheatstone quarter bridge circuit was used for strain measurement. The load cell was of length 20 mm, outer diameter 17 mm and wall thickness 1.3 mm. The degree of bending of the load cell was determined by the difference in axial strain between the gauges and was found to be less than 20 % of the mean value throughout each test. We conclude that bending of the load cell was negligible. The mean response of the gauges was used to calculate the transverse clamping force T of the specimens, and this transverse force was recorded by a data-logger. The clamping pre-load T_0 and the evolution of the load T during the test were measured and are reported below.

3. Observed failure modes

We begin by summarising the observed failure modes. The active failure mode of the bolted joint as a function of joint geometry and of clamping pre-load was determined by a combination of visual observation and X-ray CT microscopy[3]. A failure map was created for a bolted joint with zero clamping pre-load, $T_0 = 0$, as shown in Fig. 2; the location of the boundaries between failure mechanisms are derived in a subsequent section. The competing failure mechanisms for $T_0 = 0$ are shear of the bolt, tensile failure of the 0^o plies at the sides of the hole and shear failure of the laminate; these are sketched in the inserts of Fig. 2. For the case of pin loading with clamping washers absent, the shear mode of failure was replaced by a bearing mode of failure. Figure 2 is valid for clamped specimens of low *d/t* ratio. The failure map was constructed for the choice *d*=8mm and *t*=6.5mm. Further work is needed in order to determine the failure map for the clamped specimen at large *d/t* to determine whether bearing failure intervenes. This is beyond the scope of the present study. The failure map in Fig. 2 is consistent with that of Smith et al. (1986) for 0/90 CFRP laminates: they also found that shear failure dominates the map for low values of *w/d* and *b/d*.

An additional failure mechanism was observed in the present study, that of a transverse plate-buckling mode for plates of large ligament width *w*, and this is detailed below. Table 1 gives an overview of the dimensions, confinement and the corresponding failure modes observed in the experiments.

3.1 Shear failure

The shear mode of failure occurs for the clamped case, $T_0 \geq 0$, in specimens of small ligament width and height. Interrupted tests and X-ray CT observations were performed in order to reveal the deformation within the 0^o plies, 90^o plies and the delamination between plies. An idealised view of this deformation mode is sketched in Fig. 3; the accompanying interrupted test (and CT images) are reported in Fig. 4 for the clamped case with $T_0 = 0$, and of geometry b = 4

[3] Nikon X-Tek XT H 225ST, at an operating voltage of 50kV

mm, w = 6 mm and t = 12 mm. The initial undeformed state of a representative 0° ply and 90° ply is sketched in Fig. 3(a) and is labelled as (1) in the CT images of Fig 4(b) and also in the CT image of Fig. 4(c). The specimen was loaded to peak load and then fully unloaded, to obtain the point (2) on the force F versus displacement u curve of the joint in Fig. 4(a); CT scans of representative 0° plies and 90 ° plies are given in Fig. 4(b) (again labelled (2)). Reloading and subsequent unloading brought the specimen to state (3) as marked in Fig. 3, with the observed deformation state given in Fig. 4. The bolt washers prevent thickening of the specimen adjacent to the bolt, and shear failure of the 0° plies occurs. This is clear from the transverse section of the specimen in Fig. 4(c).

A simple kinematic representation of this failure mode is given in Fig. 3(b), and is described as follows. A portion *B* of 0° ply material translates by the same displacement u as that of the loading bolt. The remainder of the ply (labelled portion *A*) remains stationary, and so the collapse mechanism of the 0° ply comprises sliding by a displacement u along two splits (located at the boundary between portions *A* and *B*). The deformation state of the 90° ply is slightly more complex. A portion *C* is undeformed, whereas the portion *E* of the 90° ply remains bonded to the adjacent portion *B* in the 0° ply, and is thereby displaced by the displacement u. The portion *F* of the 90° ply contains the same fibres as portion *E*, and undergoes in-plane shear as sketched, and as shown in Fig. 4(b). The portion *F* delaminates and slides with respect to the adjacent portion *A* of the 0° ply, thereby creating a delamination patch *D*.

Now consider the case of pin loading with the clamping washers absent, for the same geometry of b = 4 mm, w = 6 mm and t = 12 mm. The force F versus displacement u curve of the joint is included in Fig. 4(a), and labelled '*free*'. A *bearing failure* occurs for this case of unconstrained out-of-plane expansion of the laminate, see the cross-section of state (3) in Fig. 4(c). The portion *B* of 0° plies and portion *E* of 90° plies (as defined in Fig. 3) undergo out-of-plane microbuckling with intermittent delamination, see Fig. 4(c).

3.2 Competing collapse modes for the clamped case, $T_0 \geq 0$

An alternative failure mode is tensile failure of the 0º plies adjacent to the loaded bolt. This has been reported previously by Attwood et al. (2014). Bolt shear intervenes for a joint of high aspect ratio b/d and w/d. A more surprising mode that is observed in the present study is out-of-plane plate-buckling for large w/d, as shown in Fig. 5. The buckling failure mode dictates the peak load and occurs shortly before the load maximum, see the dashed line in Fig. 7(b). It is conjectured that this is due to the build-up of a large tensile stress in the 90º plies above the hole leading to compression stress beneath the hole during the later stages of bolt pull-out in the shear failure mode.

4. Sensitivity of joint strength to geometry and clamping

4.1 Effect of initial clamping

The effect of initial clamping pre-load T_0 upon the axial force F versus bolt displacement u is given in Fig. 6(a) for the choice b = 4 mm, w = 6 mm and t = 6.5 mm. This choice of geometry ensures that the shear mode of failure is active. The evolution of transverse clamping force T in each test is summarised in Fig. 6(b). The main features are as follows. Delamination between the 0º and 90º plies, as labelled zone D of Fig. 3(b), occurs at a very low load of below 2 kN, and the subsequent response is linear up to the peak load, labelled F_m. The magnitude F_m increases (linearly) with the pre-load T_0 as shown in Fig. 6(c). This is explained by the pressure dependence of UHMWPE fibre composites, as discussed by Attwood et al. (2014). The clamping force T also increases to a peak value of T_m with increasing bolt displacement u. The clamping force resists out-of-plane swelling of the laminate, and for completeness Fig. 6(c) contains a plot of F_m versus T_m: again the relationship is linear. We note in passing that the peak load F_m occurs at the same value of bolt displacement, and the shift in clamping force (T_m-T_0) is constant for all specimens of a given geometry. This is consistent with the notion that the kinematics of the shear failure is insensitive to the level of clamping force.

4.2 Effect of ligament height

The effect of ligament height b upon the bolt force F versus bolt displacement u characteristic is summarised in Fig. 7(a) for 4 values of b = 2, 4, 6 and 8 mm, w = 6 mm, t = 6.5 mm and T_0 = 0. In all cases, shear failure occurred. The associated evolution of clamping force T during each test is given in Fig. 7(b). Out-of-plane swelling of the laminate leads to an increase in clamping force with increasing bolt displacement u, and a peak in the clamping force is attained at the same instant that F attains its peak value of F_m. The peak load F_m increases with increasing b, as emphasised by the plot of F_m versus b in Fig. 7(c). For completeness, this figure also contains the sensitivity of F_m to b for T_0 = 8.9 kN, for the case of a freely supported bolt (absent clamping) for which bearing failure occurs; it is clear that F_m also increases with the degree of clamping. Likewise, the peak value T_m increases with increasing degree of clamping, and increases in an almost linear manner with increasing b, see Fig. 7(d).

5. Analytical model for shear failure

An analytical model is now proposed for the observed shear failure of the bolted joint. The model assumes a collapse mechanism and thereby gives an upper bound solution for the shear failure force. First, a relation between the axial force as function of axial bolt displacement is derived for the case of relative sliding of the interface between the 0° and 90°

plies. Second, the additional force due to in-plane shearing is derived, and it is shown that this dissipation is sufficiently small for the increase in shear force to be negligible.

5.1 Plastic dissipation by inter-laminar shearing

The portion F delaminates and slides with respect to the portion A of the 0° ply, thereby creating a delamination patch D, see Fig. 3(b). The delamination patch D is divided into two zones D1 and D2, see Fig. 8. The axial bolt displacement u is related to the rotation ϕ of the 90° plies by

$$u = w \sin\phi \tag{1}$$

and the fibres are taken to be inextensible. The delamination patches D1 and D2 are of area A_1 and A_2, respectively, where

$$\begin{aligned} A_1 &= w \cos\phi \left(b + \frac{d}{2} - u\right) \\ A_2 &= \frac{1}{2}\, w \cos\phi\ u \end{aligned} \tag{2}$$

The total number of ply interfaces n_I , over which inter-laminar sliding occurs, is

$$n_I = \frac{t}{h} - 1 \tag{3}$$

where t is the specimen thickness and h is the ply thickness. Now, the principle of virtual work requires that

$$F\,\delta u = 2\,n_I\,\tau_y \left(A_1 \frac{\delta u}{2} + A_2 \frac{\delta u}{3}\right) \tag{4}$$

where δu is a virtual displacement. Here, a simple rigid-plastic constitutive relation is assumed such that τ_y is the inter-laminar shear yield strength. The factors of 1/2 and 1/3 arise from the fact that the assumed displacement field varies across the width of the delamination patch. Upon making use of Eqs. (1) and (2), the virtual work statement (4) reduces to

$$F = n_I\, \tau_y\, w \cos\phi \left(b + \frac{d}{2} - \frac{2}{3}\, w \sin\phi \right) \tag{5}$$

with peak value F_{pc} for the plastic collapse mode achieved at $\phi = 0$, such that

$$F_{pc} = n_I\, \tau_y\, w \left(b + \frac{d}{2} \right) \tag{6}$$

5.2 Additional plastic dissipation due to in-plane shearing

The additional force ΔF due to in-plane shearing is now deduced. The portion F in Fig. 3 undergoes in-plane shearing. The portion F has an in-plane area of

$$A_F = 2 \left(b + \frac{d}{2} \right) w \cos\phi \tag{7}$$

The virtual displacement δu is related to the virtual rotation $\delta\phi$ by

$$\delta u = w \cos\phi \;\; \delta\phi \tag{8}$$

Using the displacement-rotation relation, Eq. (1). During a virtual displacement, the area A_F shears an amount $\delta\phi$. Then, the additional term in the principle of virtual work for in-plane shearing is of the form

$$\Delta F\; \delta u = A_F\, h\, \delta\phi\, \tau_y\, n_{90} \tag{9}$$

where n_{90} is the number of 90° plies. Again, a simple rigid-plastic constitutive relation is used, where the in-plane shear yield strength τ_y is identical to the inter-laminar yield strength. The relation (9) is simplified via Eqs. (7) and (8) to read

$$\Delta F = 2 \left(b + \frac{d}{2} \right) \tau_y\, n_{90}\, h \tag{10}$$

Upon normalising the additional axial force ΔF due to in-plane shearing by the peak load Eq. (6) due to inter-laminar shearing we obtain

$$\frac{\Delta F}{F_{pc}} = \frac{2\left(b+\frac{d}{2}\right)}{\left(b+\frac{d}{2}\right)} \frac{n_{90}}{n_I} \frac{h}{w} \tag{11}$$

Now, the number of interfaces n_I is twice the number of 90° plies n_{90}. Consequently, the additional force arriving from in-plane shearing scales as

$$\frac{\Delta F}{F_{pc}} = \frac{h}{w} \tag{12}$$

Recall that the ply thickness h equals 60 μm and the ligament width w equals 6 mm for the majority of the test specimens. Thus, in-plane shearing will increase the axial force by only 1% and this is deemed negligible.

6. Comparison of shear failure prediction with observation

The analytical model of shear failure is now compared with the experimental results by treating the inter-laminar shear strength τ_y as a free parameter that depends upon the degree of clamping. The predictions of Eq. (6) are compared with the measured values of maximum force F_m in Fig. 7(c), assuming that τ_y = 0.95 MPa for clamping-free, τ_y = 2.2 MPa for T_0 = 0 and τ_y = 2.5 MPa for T_0 = 8.9 kN. Recall that the measured inter-laminar shear strength is τ_y = 2 MPa as obtained by Liu et al. (2014) and Attwood et al. (2014); they used a double-notch shear test. The agreement is satisfactory.

The out-of-plane clamping pressure increases the inter-laminar yield strength as follows. Attwood et al. (2014) studied the out-of-plane compressive response of UHMWPE laminates. They observed a pressure sensitivity of the form

$$\tau_y = \tau_0 + \mu p \tag{13}$$

where τ_y is the shear yield strength, τ_0 is the strength in the absence of pressure, p is the pressure and μ is a non-negative pressure sensitivity coefficient. Attwood et al. (2014) found that a coefficient $\mu = 0.05$ gave good agreement with experimental results. The increased inter-laminar yield strength as observed in the current study can be explained by the pressure sensitivity of UHMWPE. To illustrate this, consider a specimen of ligament width w = 6 mm, ligament height b = 8 mm and bolt diameter d = 8 mm. An initial pre-load of T_0 = 8.9 kN results in an average pressure p= 43 MPa beneath the clamping ring. Upon substituting an initial yield strength, τ_0 = 0.95 MPa, a pressure sensitivity coefficient μ = 0.05 and p= 43 MPa into Eq. (13) the predicted yield strength is τ_y = 3.1 MPa. This is in reasonable agreement with the inferred value of τ_y = 2.5 MPa.

7. Failure mechanism map

The background to the construction of the failure map of Fig. 2 is now given. We consider each mechanism in turn. Introduce the non-dimensional geometric parameters

$$\bar{t} = \frac{t}{d} \qquad \bar{b} = \frac{b}{d} \qquad \bar{w} = \frac{w}{d} \tag{14}$$

along with the non-dimensional force on the bolt

$$\bar{F} = \frac{F}{d\ t\ \tau_y} \tag{15}$$

where d is the bolt diameter, t the plate thickness and τ_y is the inter-laminar shear yield strength.

7.1 Shear failure

The load maximum for the shear failure is given by Eq. (6) using the simple analytical model. The non-dimensional force at shear failure (plastic collapse) is

$$\bar{F}_{pc} = \frac{F_{pc}}{d\ t\ \tau_y} = n_I\ \bar{w}\ \left(\bar{b} + \frac{1}{2}\right)\frac{1}{\bar{t}} \tag{16}$$

7.2 Bolt shear

The bolt carries a transverse shear force $V = F/2$ at two locations. Assume that the bolt shears plastically when the shear stress on the section attains the shear strength τ_{bf} . High strength bolts are almost elastic, ideally plastic in their response, with a tensile strength of σ_{bf} = 1200 MPa, and a shear strength τ_{bf} = 1200/$\sqrt{3}$ MPa = 693 MPa by the von Mises yield criterion. Consequently, bolt shear occurs at a load

$$F_{bf} = \frac{\pi}{2} d^2\ \tau_{bf} \tag{17}$$

and, upon introducing the non-dimensionalisation we obtain

$$\bar{F}_{bf} = \frac{F_{bf}}{d\ t\ \tau_y} = \frac{\pi}{2}\ \frac{\tau_{bf}}{\tau_y}\frac{1}{\bar{t}} \tag{18}$$

7.3 Tensile failure of the laminate

Tensile failure of the fibres within the 0° plies occurs at an axial stress of σ_f = 3000 MPa within the fibres. Recall that the strength of the composite normal to the fibre direction is three orders of magnitude lower than in the direction of the fibres and is thereby negligible. The strength of the composite in tension is

$$\sigma_t = \frac{1}{2}\sigma_f\ c^f \tag{19}$$

where c^f = 0.83 is the volume fraction of fibres (Liu et al. (2014)). A factor of 1/2 is introduced due to the equal volume fraction of 0° and 90° plies, and the fact that the 90° plies provide a negligible contribution to the strength. The smallest cross sectional area normal to the force F is $2\ w\ t$, see Fig. 1. Consequently, the force at tensile failure is

$$F_t = 2\, w\, t\, \sigma_t \tag{20}$$

and so the non-dimensional force $\bar{F}_0$ at tension failure is

$$\bar{F}_t = \frac{F_t}{d\, t\, \tau_y} = 2\, \frac{\sigma_t}{\tau_y}\, \bar{w} \tag{21}$$

7.4 Construction of failure map

A failure map for T_0 = 0 is constructed with geometric axes b/d and w/d in order to identify regimes of dominance of the competing failure modes, see Fig. 2. The active mode has the lowest failure load from the relations Eq. (16), (18) and (21). The boundaries are located by equating the failure load of competing mechanisms. The precise boundary between shear failure and out-of-plane plate buckling is unknown; consequently, the boundary is not drawn in the failure map.

8. Concluding remarks

The present study highlights the dominance of the shear mode of joint failure in a bolted joint made from a UHMWPE laminate, and subjected to out-of-plane clamping by the bolt. The 0^{o} plies split such that the central portion of 0^{o} plies (adjacent to the bolt) is sheared-out from the joint by movement of the bolt. The 90^{o} plies that are stacked with the central portion of 0^{o} plies are also dragged-out of the joint by the bolt displacement. This leads to tensile pull-through of the 90^{o} plies and to delamination of the 0^{o} plies.

The strength at shear failure is increased substantially by increasing clamping force, and this is explained in terms of the pressure sensitivity of the shear strength of the UHMWPE composite. A simple analytical model highlights the importance of slip between the plies in providing the resistance to a shear failure. Also, a failure map is constructed and provides useful guidelines for joint strength as a function of geometry. In order to predict the plate buckling mode at large ligament width w, a 3D finite element model would be required and this is beyond the scope of the present study.

Acknowledgements

The research work was supported by the Thomas B. Thriges Fond; Aage og Johanne Louis-Hansens Fond; Knud Højgaards Fond; Augustinus Fonden; Reinholdt W Jorck og Hustrus Fond; Marie & M. B. Richters Fond; and the Graduate School of Science and Techonology (Aarhus University). The authors are grateful for financial support for this work in the form of an ERC MULTILAT grant 669764, and to DSM for providing the Dyneema® composites used in this study.

References

Attwood, J.P., Fleck, N.A., Wadley, H.N.G., Deshpande, V.S., (2015). The compressive response of ultra-high molecular weight polyethylene fibres and composites. Int. J. Solids Struct. 71, 141–155. https://doi.org/10.1016/j.ijsolstr.2015.06.015

Attwood, J.P., Khaderi, S.N., Karthikeyan, K., Fleck, N.A., Omasta, M.R., Wadley, H.N.G., Deshpande, V.S., (2014). The out-of-plane compressive response ofDyneema ®composites. J. Mech. Phys. Solids 70, 200–226. https://doi.org/10.1016/j.jmps.2014.05.017

Camanho, P., Matthews, F., (1997). Stress analysis and strength prediction of mechanically fastened joints in FRP: A review. Compos. Part A Appl. Sci. Manuf. 28, 529–547. https://doi.org/10.1016/S1359-835X(97)00004-3

Govaert, L.E., Lemstra, P.J., (1992). Deformation behavior of oriented UHMW-PE fibers.

Colloid Polym. Sci. 270, 455–464. https://doi.org/10.1007/BF00665989

Govaert, L.E., Peijs, T., (1995). Tensile strength and work of fracture of oriented polyethylene fibre. Polymer (Guildf). 36, 4425–4431. https://doi.org/10.1016/0032-3861(95)96848-3

Grujicic, M., Arakere, G., He, T., Bell, W.C., Glomski, P.S., Cheeseman, B.A., (2009). Multi-scale ballistic material modeling of cross-plied compliant composites. Compos. Part B Eng. 40, 468–482. https://doi.org/10.1016/j.compositesb.2009.02.002

Iannucci, L., Pope, D., (2011). High velocity impact and armour design. Express Polym. Lett. 5, 262–272. https://doi.org/10.3144/expresspolymlett.2011.26

Karthikeyan, K., Russell, B.P., Fleck, N.A., O'Masta, M., Wadley, H.N.G., Deshpande, V.S., (2013). The soft impact response of composite laminate beams. Int. J. Impact Eng. 60, 24–36. https://doi.org/10.1016/j.ijimpeng.2013.04.002

Koh, A.C.P., Shim, V.P.W., Tan, V.B.C., (2010). Dynamic behaviour of UHMWPE yarns and addressing impedance mismatch effects of specimen clamps. Int. J. Impact Eng. 37, 324–332. https://doi.org/10.1016/j.ijimpeng.2009.10.008

Liu, B.G., Kandan, K., Wadley, H.N.G., Deshpande, V.S., (2018). Deep penetration of ultra-high molecular weight polyethylene composites by a sharp-tipped punch. J. Mech. Phys. Solids. https://doi.org/10.1016/j.jmps.2018.06.001

Liu, G., Thouless, M.D., Deshpande, V.S., Fleck, N.A., (2014). Collapse of a composite beam made from ultra high molecular-weight polyethylene fibres. J. Mech. Phys. Solids 63, 320–335. https://doi.org/10.1016/j.jmps.2013.08.021

Russell, B.P., Karthikeyan, K., Deshpande, V.S., Fleck, N.A., (2013). The high strain rate response of Ultra High Molecular-weight Polyethylene: From fibre to laminate. Int. J. Impact Eng. 60, 1–9. https://doi.org/10.1016/j.ijimpeng.2013.03.010

Smith, P., Lemstra, P.J., (1980). Ultra-high strength polyethylene filaments by solution spinning/drawing. 3. Influence of drawing temperature. Polym. (United Kingdom) 21, 1341–1343. https://doi.org/10.1016/0032-3861(80)90205-0

Smith, P.A., Pascoe, K.J., Polak, C., Stroud, D.O., (1986). The behaviour of single-lap bolted joints in CFRP laminates. Compos. Struct. 6, 41–55. https://doi.org/10.1016/0263-8223(86)90067-X

Thoppul, S.D., Finegan, J., Gibson, R.F., (2009). Mechanics of mechanically fastened joints in polymer-matrix composite structures - A review. Compos. Sci. Technol. 69, 301–329. https://doi.org/10.1016/j.compscitech.2008.09.037

Wilding, M.A., Ward, I.M., (1978). Tensile creep and recovery in ultra-high modulus linear polyethylenes. Polymer (Guildf). 19, 969–976. https://doi.org/10.1016/0032-3861(78)90208-2

Table Captions

Table 1. Dimensions, confinement and observed failure modes

Figure Captions

Fig. 1 (a) Specimen geometry. All dimensions are in mm. **(b)** Experimental set-up. A three-dimensional view is shown on the left. A sectional view of the top part is shown on the right. All dimensions are in mm.

Fig. 2 Failure map for the choice $T_0 = 0$. Laminate thickness $t/d = 0.8$ and ply thickness $h/d = 0.0075$.

Fig. 3. The load transfer mechanism for shear failure of the bolted joint, with $T_0 \geq 0$. D denotes delamination between the [0°/90°] plies.

Fig. 4 (a) Axial force F versus axial displacement u for the choice $T_0 = 0$ and the unconstrained case (Free). For both tests, $b = 4\ mm$, $w = 6\ mm$ and $t = 12\ mm$. **(b)** CT images of selected 90° or 0° plies near the mid-plane of the specimen, for the choice $T_0 = 0$. Plan view along the x_3 direction of Fig. 1. **(c)** Transverse views of the shear failure of the plies above the pin for the clamped case with $T_0 = 0$, and for the pin-loaded case, labelled free.

Fig. 5. Optical image of specimen of width $w = 25\ mm$, $b = 4\ mm$, $t = 6.5\ mm$, showing failure by buckling of plate beneath the pin.

Fig. 6 (a) Axial force F versus axial displacement u. **(b)** Transverse force T versus axial displacement u. **(c)** Maximum axial force F_m versus initial transverse force T_0 and maximum value T_m. Dashed lines are best fits to the data. Throughout, specimen ligament height $b = 4\ mm$, width $w = 6\ mm$ and laminate thickness $t = 6.5\ mm$.

Fig. 7 (a) Axial force F versus axial displacement u for the choice $T_0 = 0$. **(b)** Transverse force T versus axial displacement u for the choice $T_0 = 0$. **(c)** Maximum axial force F_m/w versus ligament height b. Solid lines show predictions by the analytical model. **(d)** Maximum transverse force T_m/w versus ligament height b. Dashed lines show best fit to the data. Throughout, specimen $w = 6\ mm$, thickness $t = 6.5\ mm$ besides an experiment showing buckling with $w = 25\ mm$ (dashed line).

Fig. 8. Sketch of the geometry for analytical model.

Table 1. Dimensions, confinement and observed failure modes

t, mm	d, mm	b, mm	w, mm	Bolt pre-load T_0, kN	Failure mode
12	6	15	7	free	Bolt shear
6.5	6	40	3	0	Tension
6.5	6	4	25	0	Buckling
12	8	4	6	0	Shear
12	8	4	6	free	Shear
6.5	8	4	6	0	Shear
6.5	8	4	6	0.84	Shear
6.5	8	4	6	2.89	Shear
6.5	8	4	6	3.67	Shear
6.5	8	4	6	4.75	Shear
6.5	8	4	6	6.59	Shear
6.5	8	4	6	7.67	Shear
6.5	8	4	6	8.92	Shear
6.5	8	2	6	free	Shear
6.5	8	4	6	free	Shear
6.5	8	6	6	free	Shear
6.5	8	8	6	free	Shear
6.5	8	2	6	0	Shear
6.5	8	4	6	0	Shear
6.5	8	6	6	0	Shear
6.5	8	8	6	0	Shear
6.5	8	2	6	8.92	Shear
6.5	8	4	6	8.92	Shear
6.5	8	6	6	8.92	Shear
6.5	8	8	6	8.92	Shear

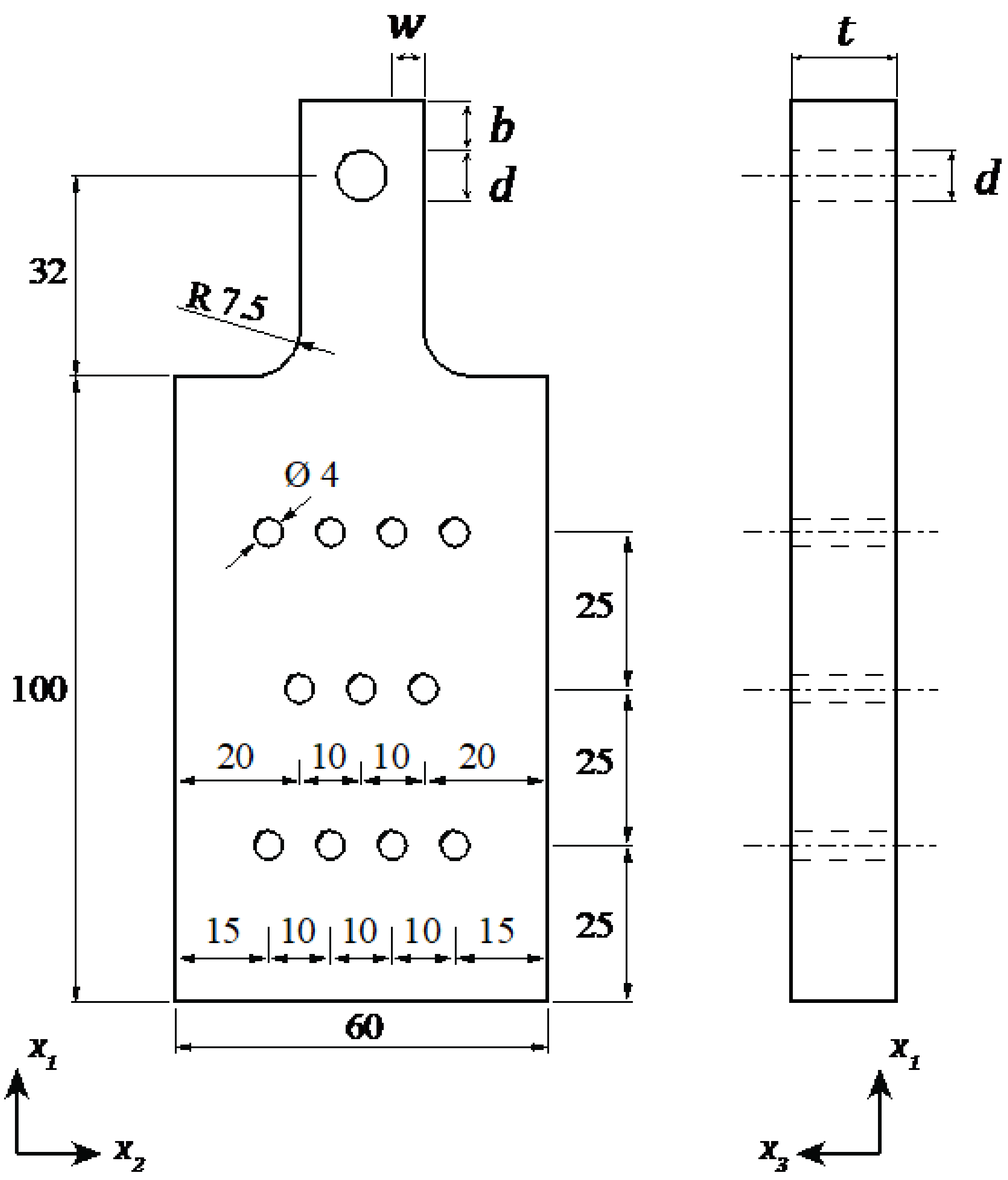

Fig. 1(a). Specimen geometry. All dimensions are in mm.

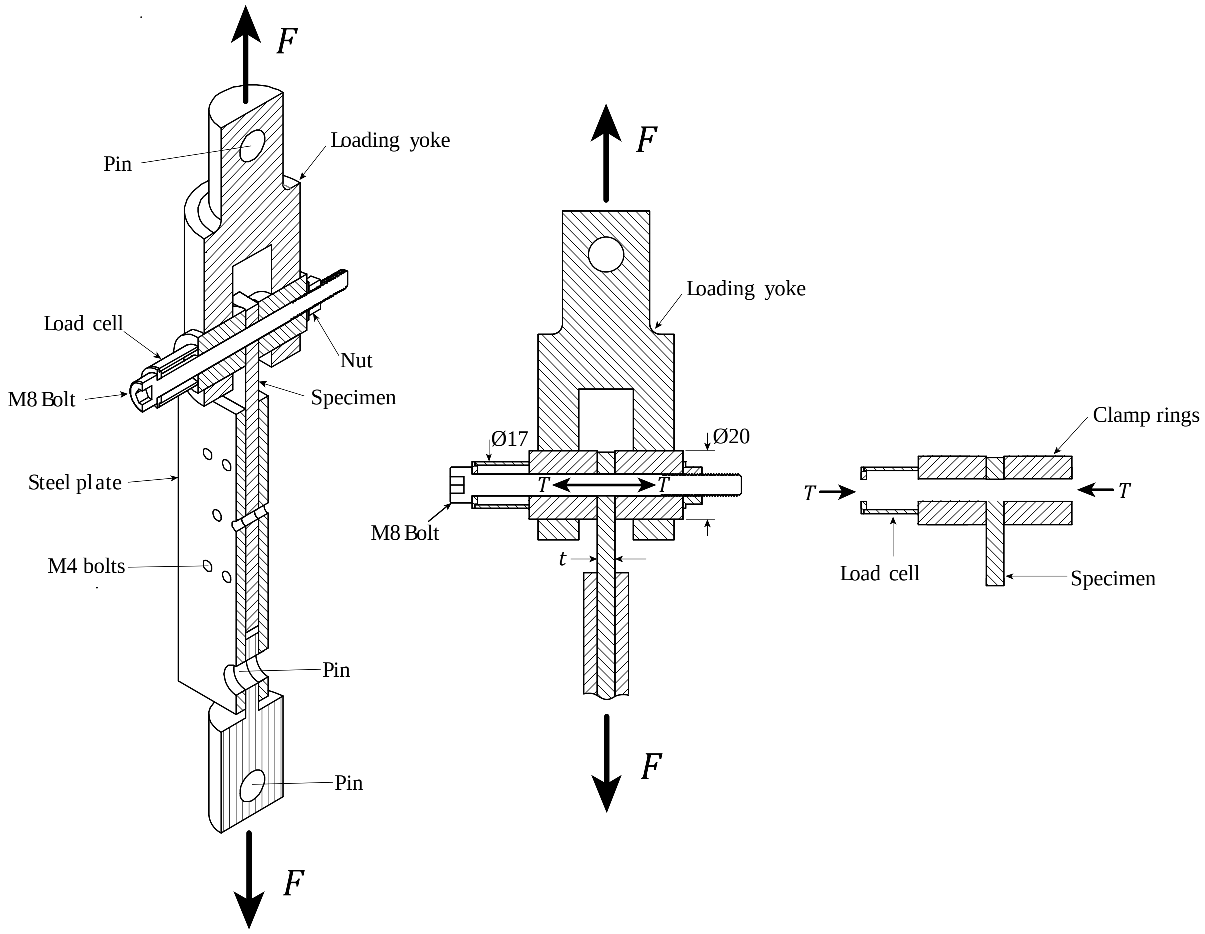

Fig. 1(b). Experimental set-up. A three-dimensional view is shown on the left. A sectional view of the top part is shown on the right. All dimensions are in mm.

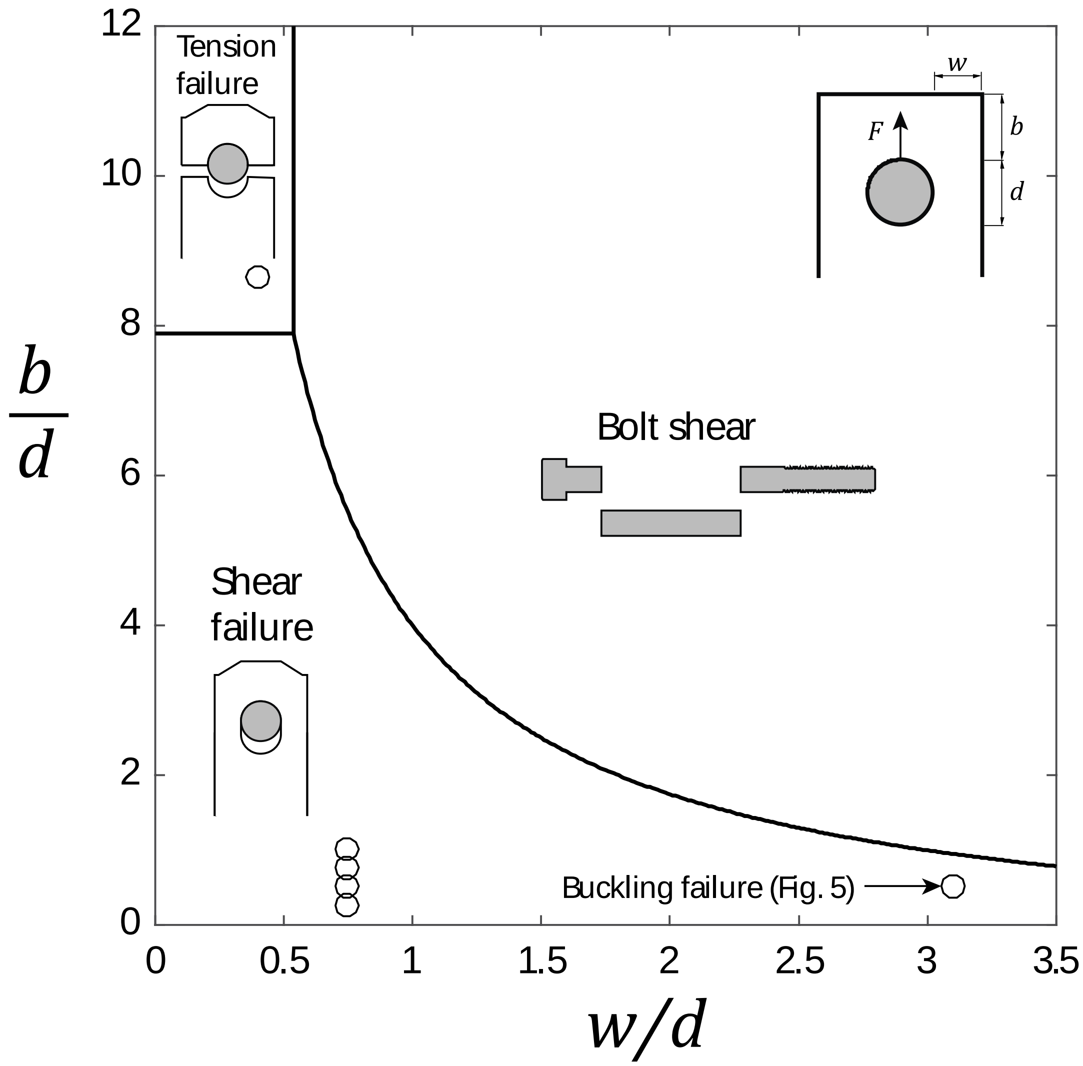

Fig. 2 Failure map for the choice $T_0 = 0$. Laminate thickness $t/d = 0.8$ and ply thickness $h/d = 0.0075$.

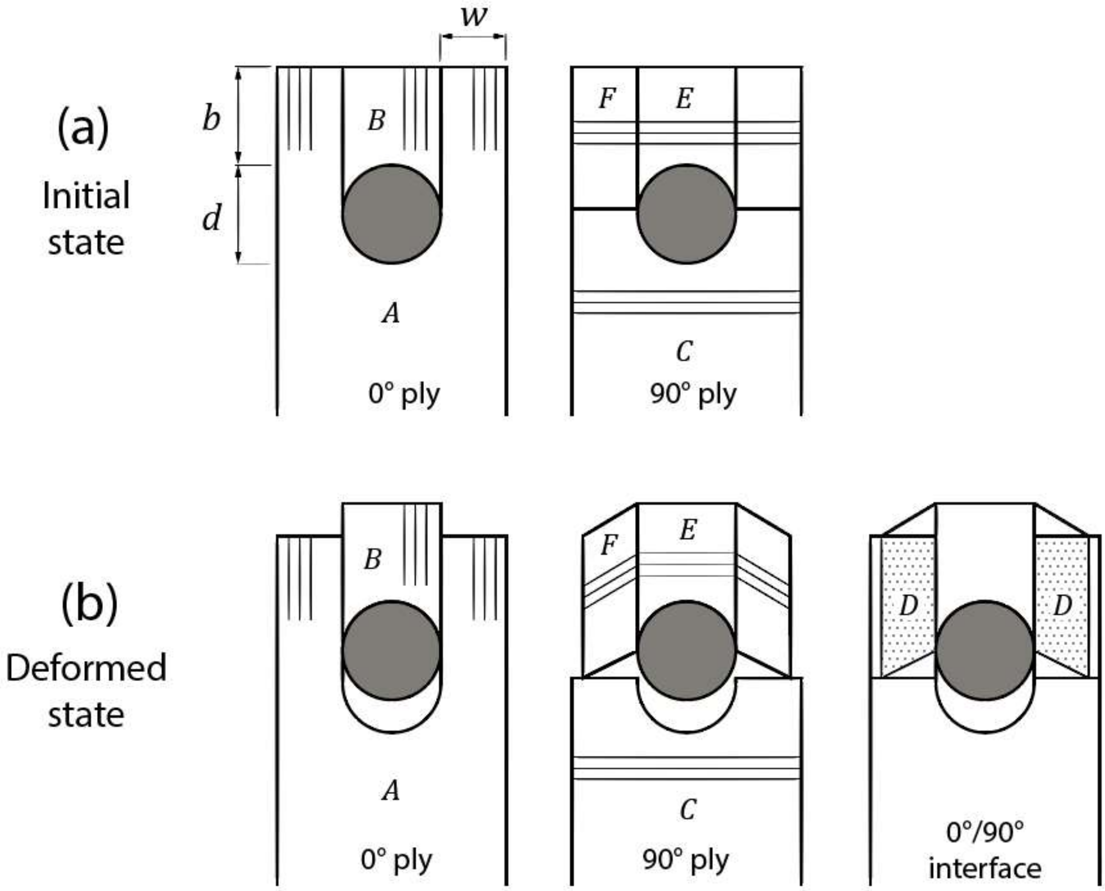

Fig. 3. The load transfer mechanism for shear failure of the bolted joint, with $T_0 \geq 0$. D denotes delamination between the [0°/90°] plies.

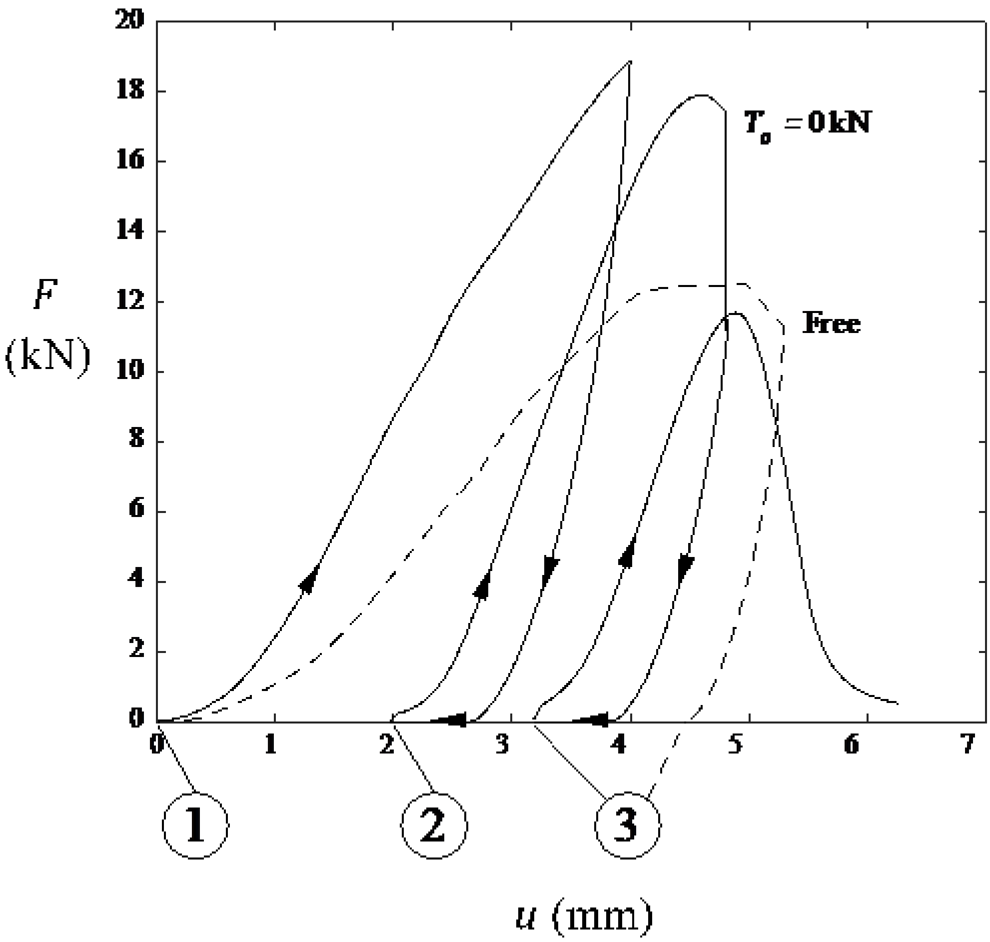

Fig. 4(a). Axial force F versus axial displacement u for the choice $T_0 = 0$ and the unconstrained case (Free). For both tests, $b = 4\ mm$, $w = 6\ mm$ and $t = 12\ mm$.

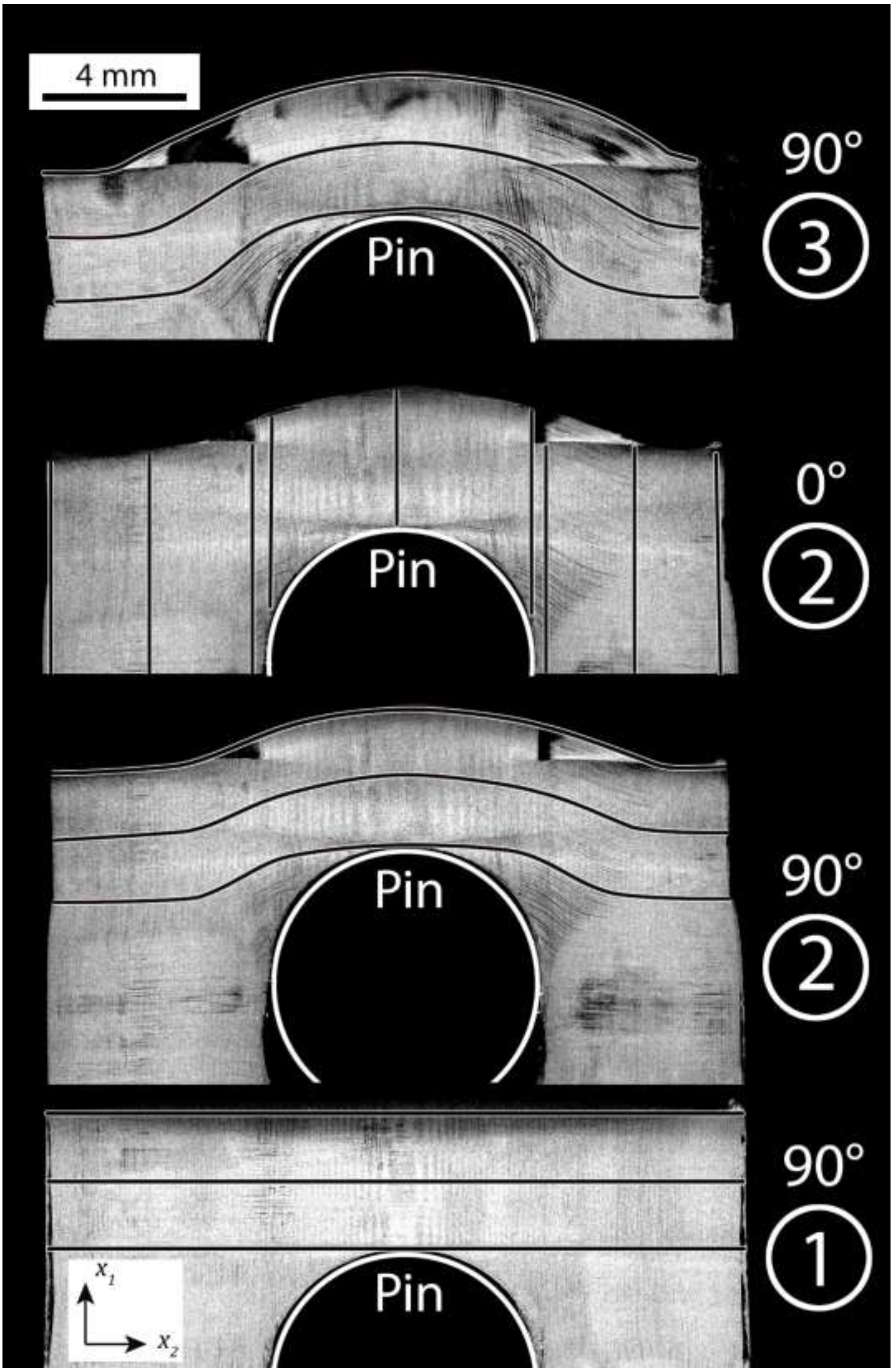

Fig. 4(b). CT images of selected 90° or 0° plies near the mid-plane of the specimen, for the choice $T_0 = 0$. Plan view along the x_3 direction of Fig. 1.

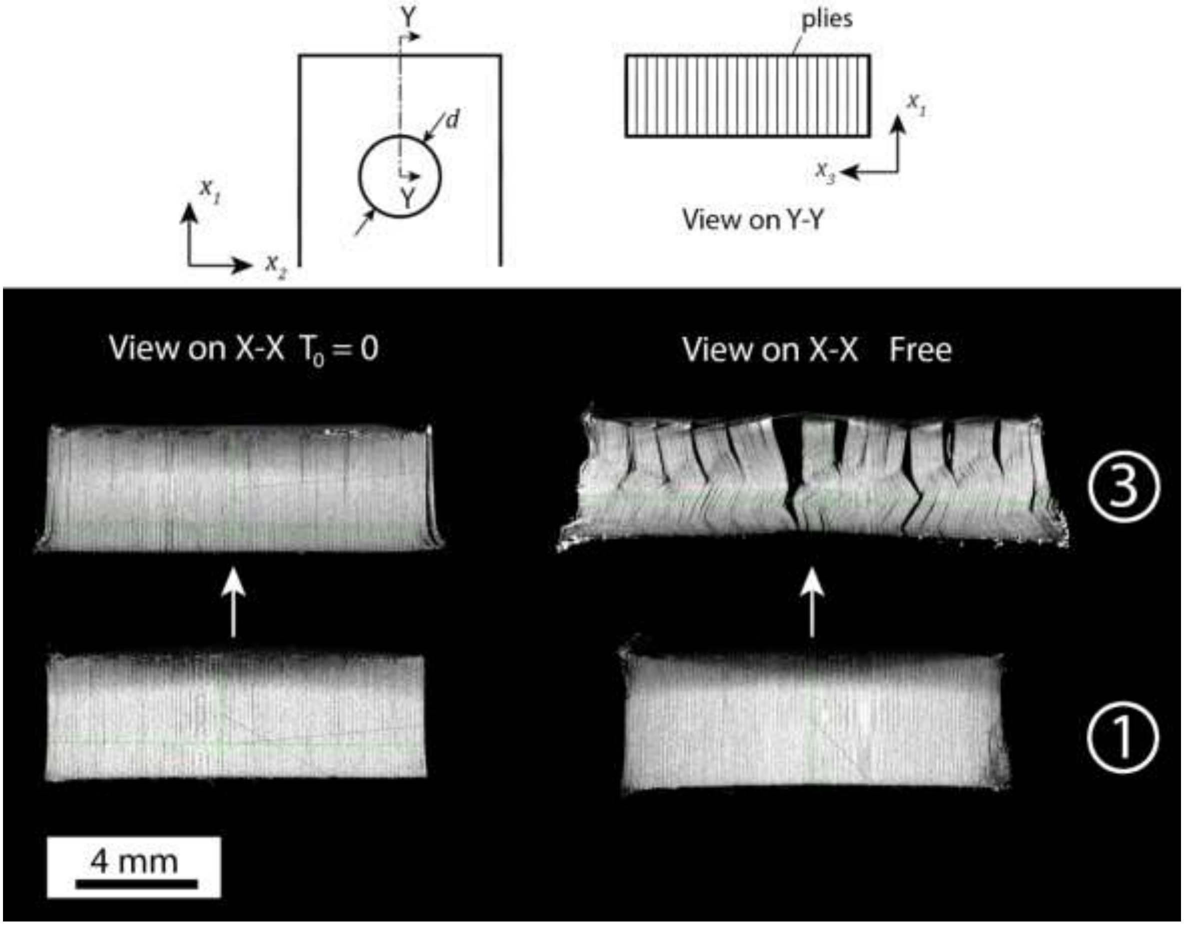

Fig. 4(c). Transverse views of the shear failure of the plies above the pin for the clamped case with $T_0 = 0$, and for the pin-loaded case, labelled free.

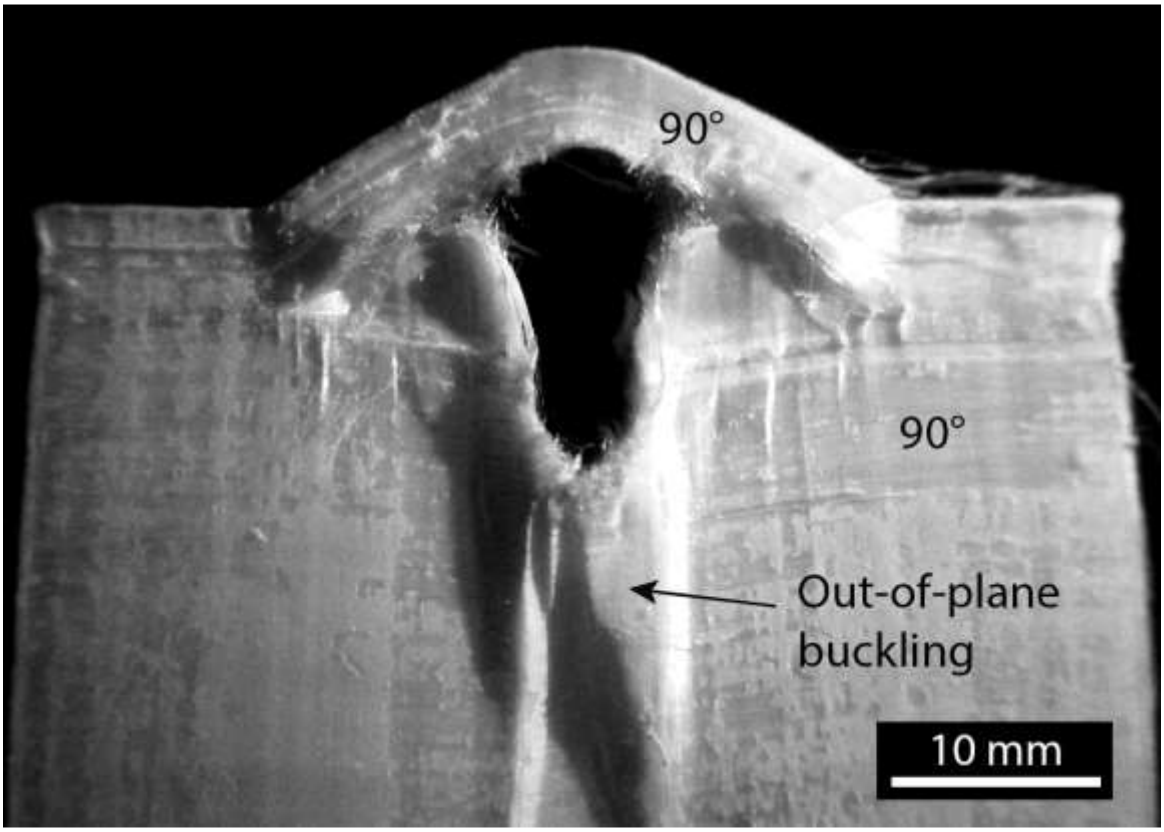

Fig. 5. Optical image of specimen of width $w = 25\ mm$, $b = 4\ mm$, $t = 6.5\ mm$, showing failure by buckling of plate beneath the pin.

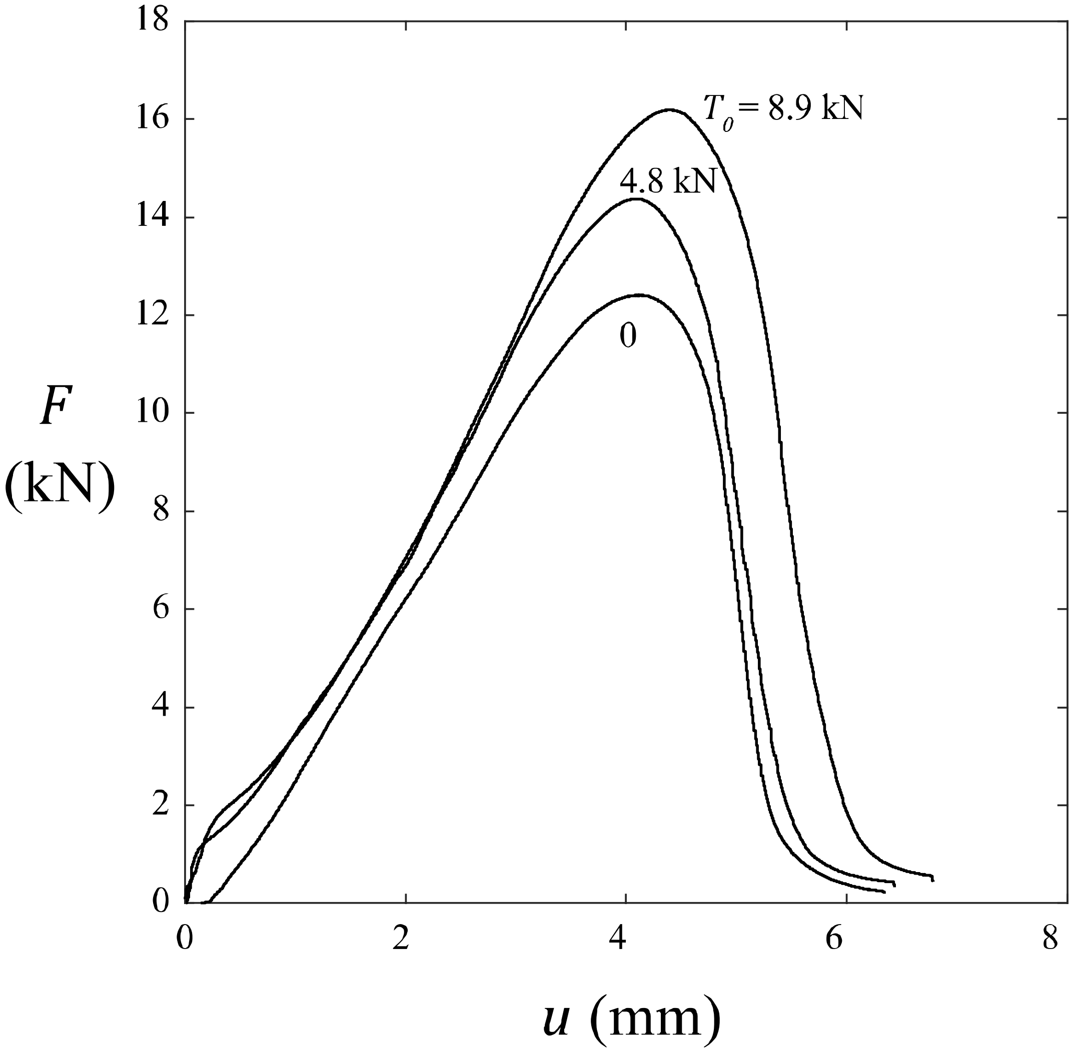

Fig. 6(a). Axial force F versus axial displacement u.

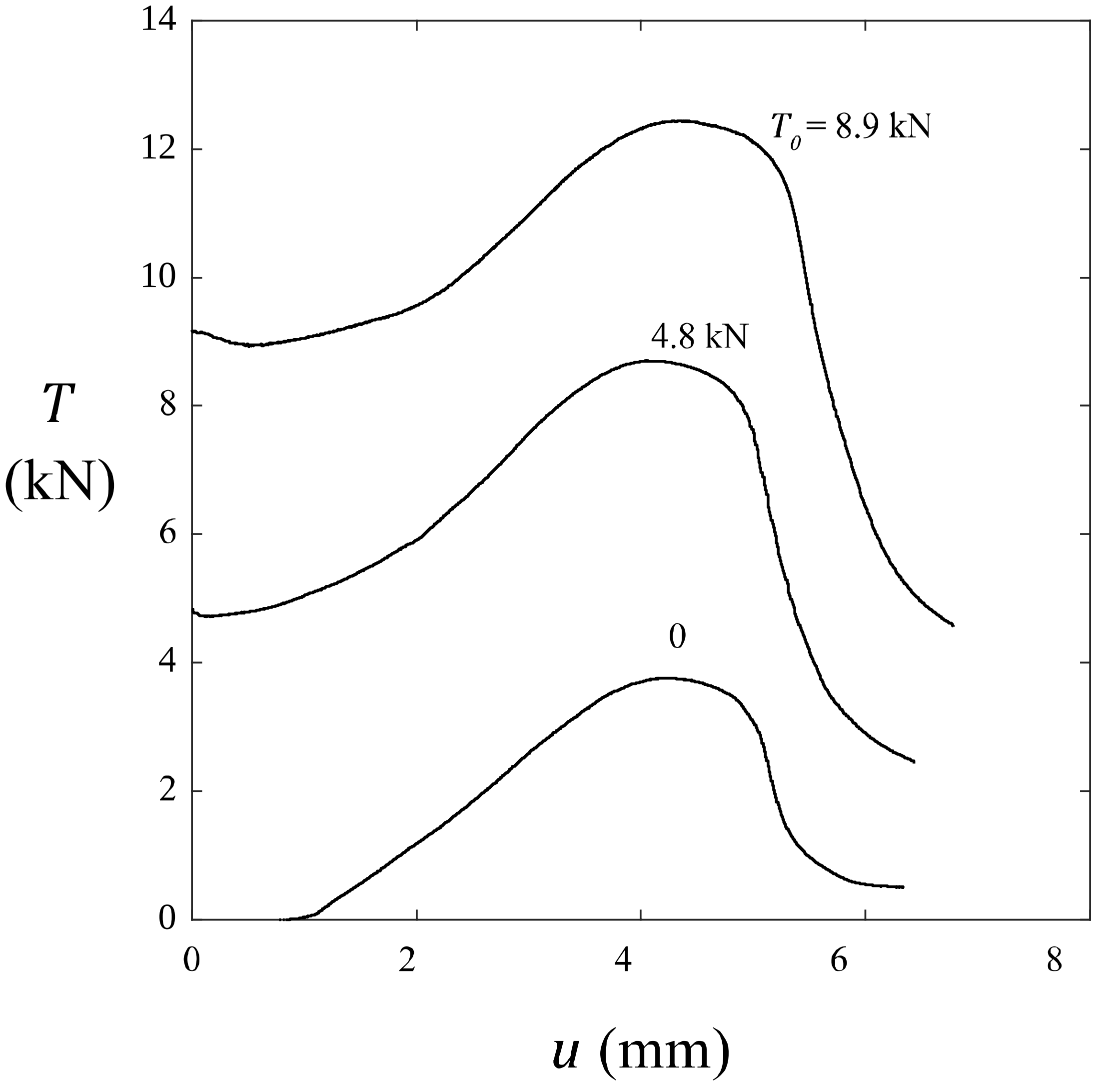

Fig. 6(b). Transverse force T versus axial displacement u.

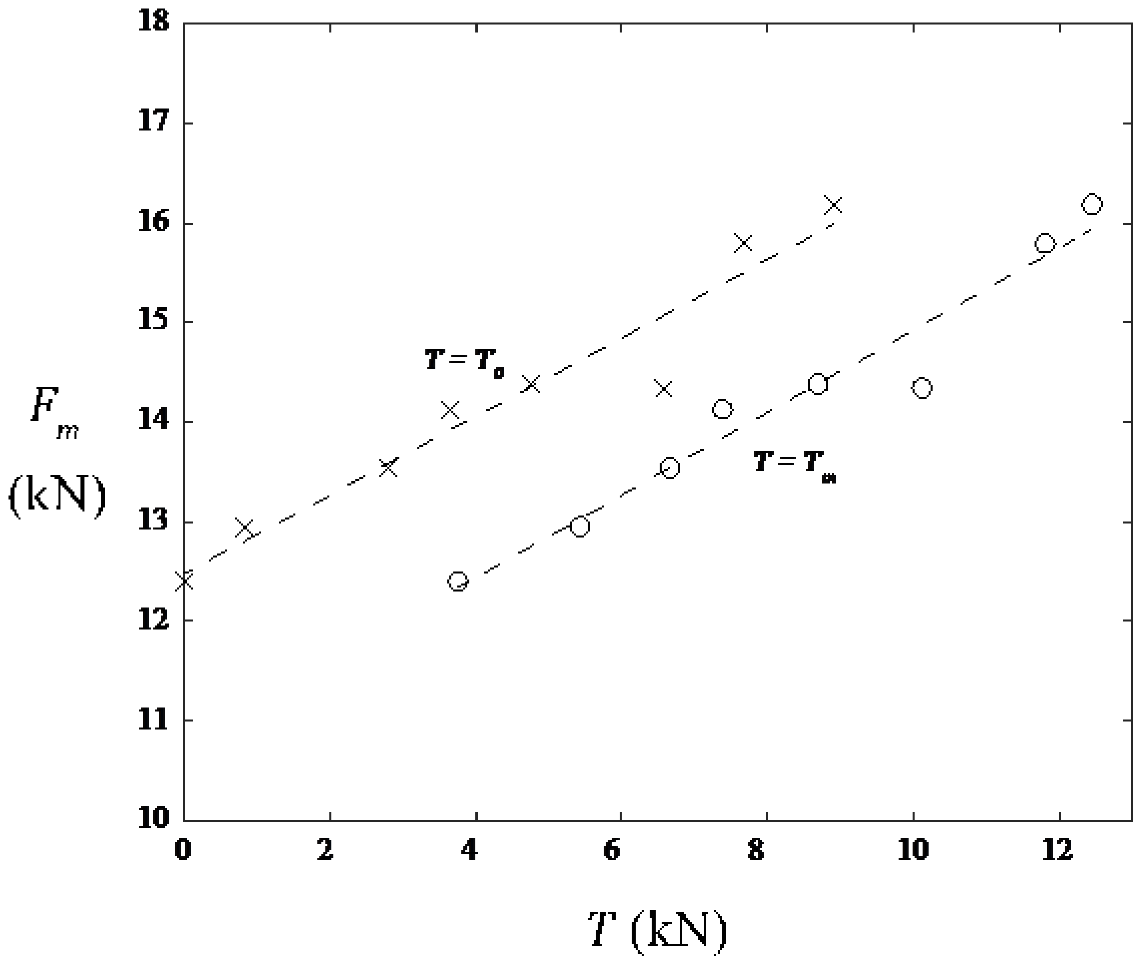

Fig. 6(c). Maximum axial force F_m versus initial transverse force T_0 and maximum value T_m. Dashed lines are best fits to the data. Throughout, specimen ligament height $b = 4\ mm$, width $w = 6\ mm$ and laminate thickness $t = 6.5\ mm$.

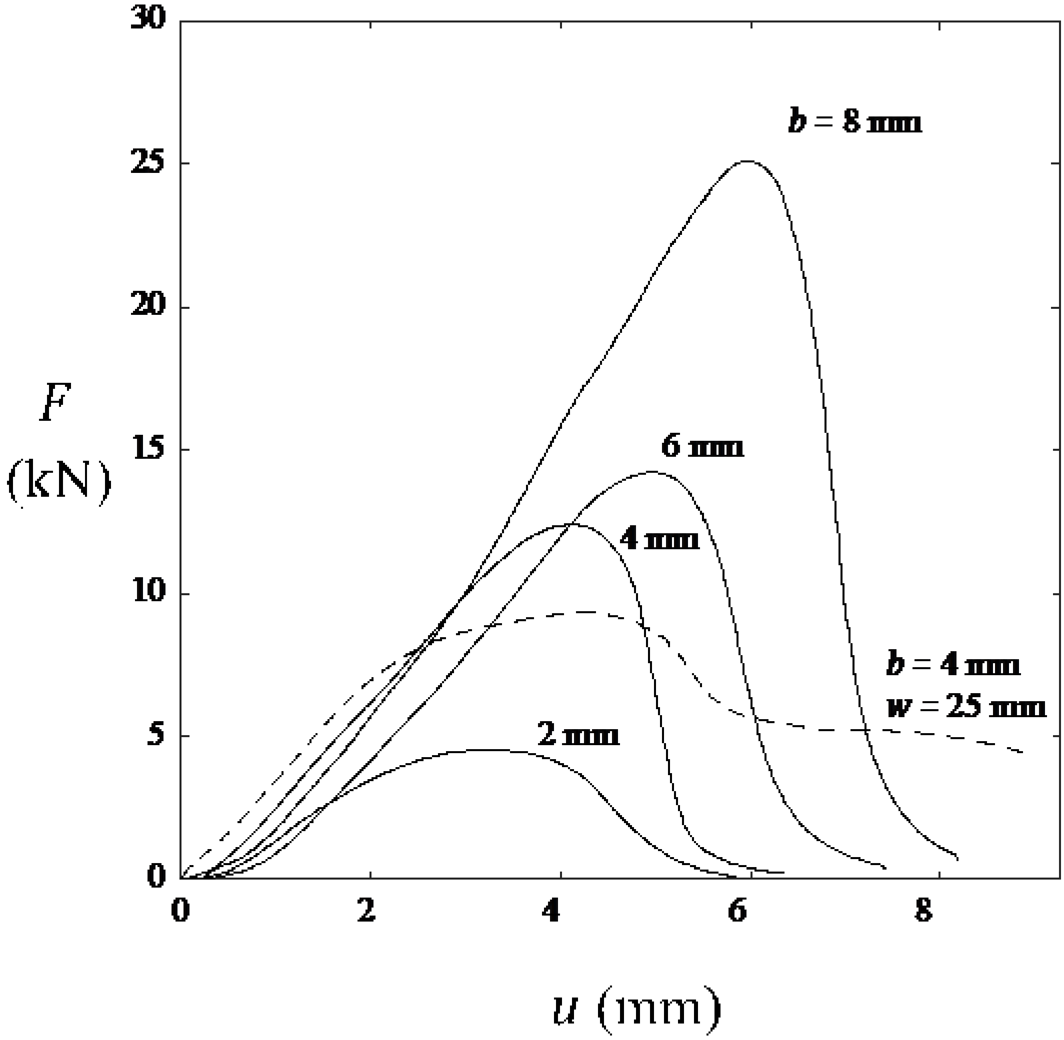

Fig. 7(a). Axial force F versus axial displacement u for the choice $T_0 = 0$.

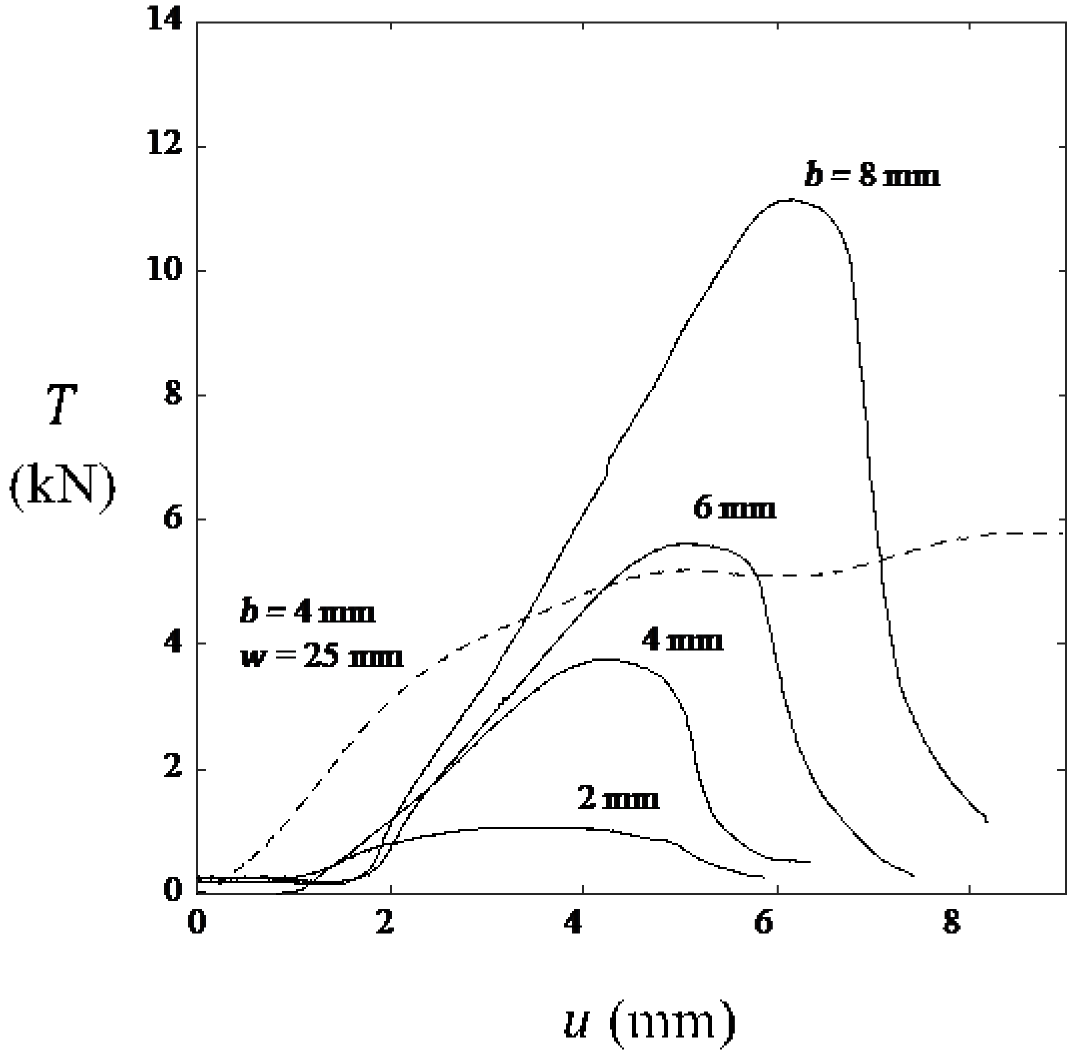

Fig. 7(b). Transverse force T versus axial displacement u for the choice $T_0 = 0$.

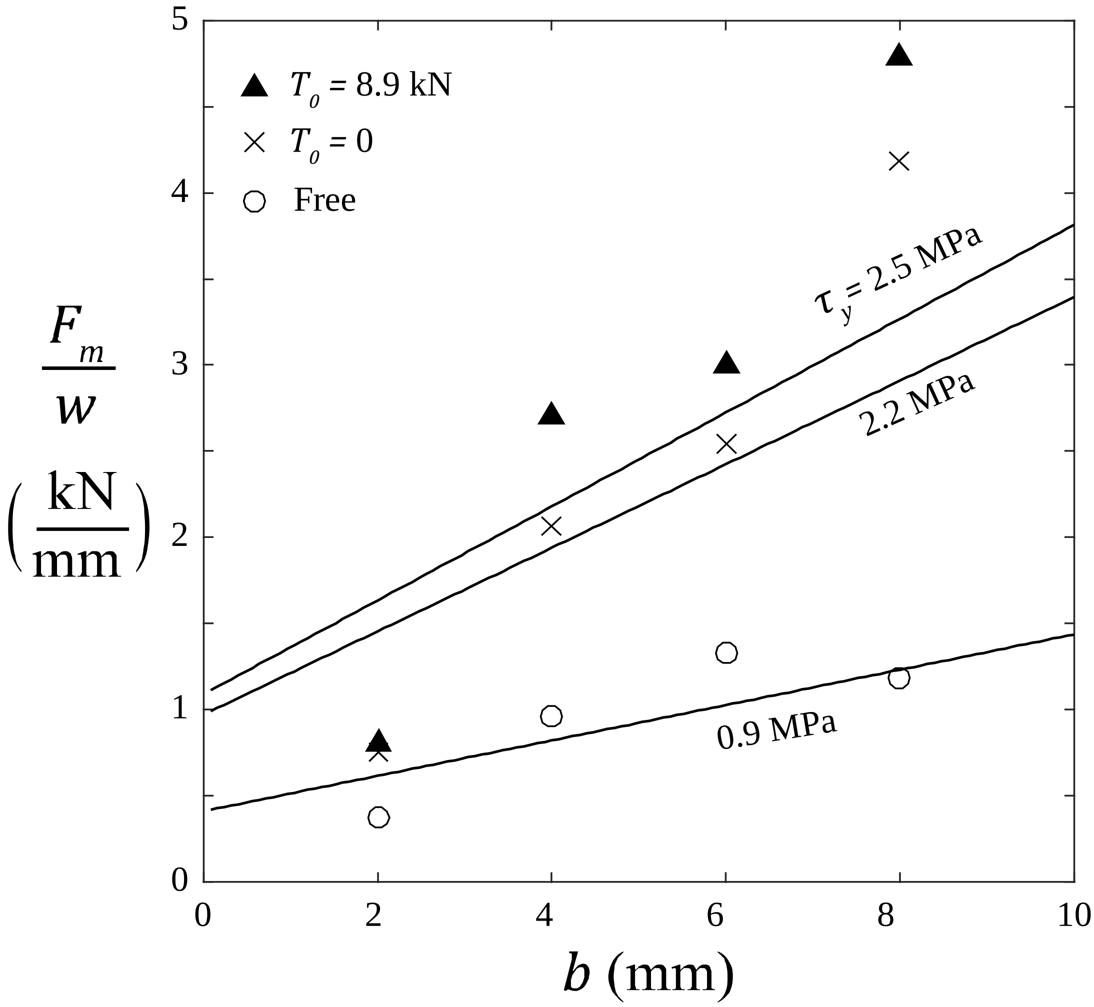

Fig. 7(c). Maximum axial force F_m/w versus ligament height b. Solid lines show predictions by the analytical model.

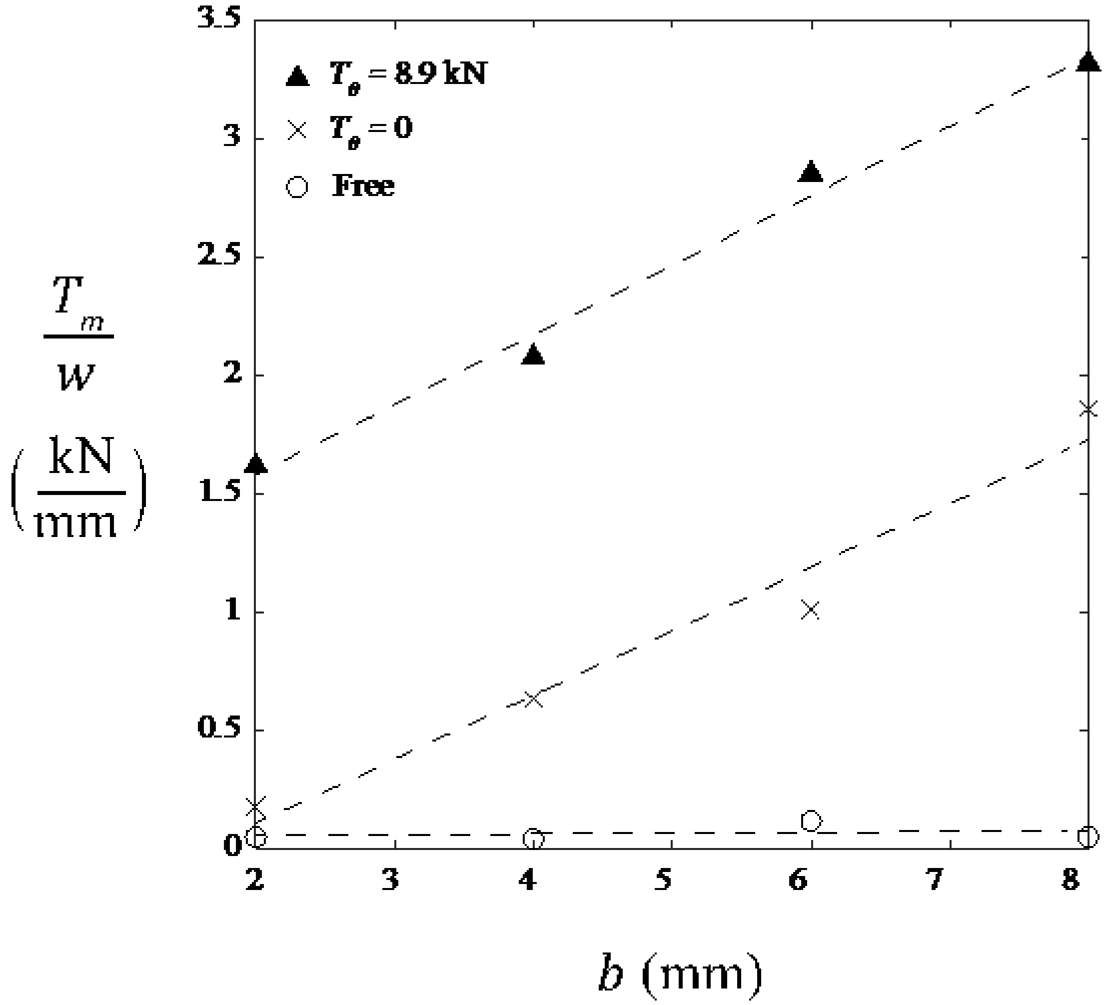

Fig. 7(d). Maximum transverse force T_m/w versus ligament height b. Dashed lines show best fit to the data. Throughout, specimen $w = 6\ mm$, thickness $t = 6.5\ mm$ besides an experiment showing buckling with $w = 25\ mm$ (dashed line).

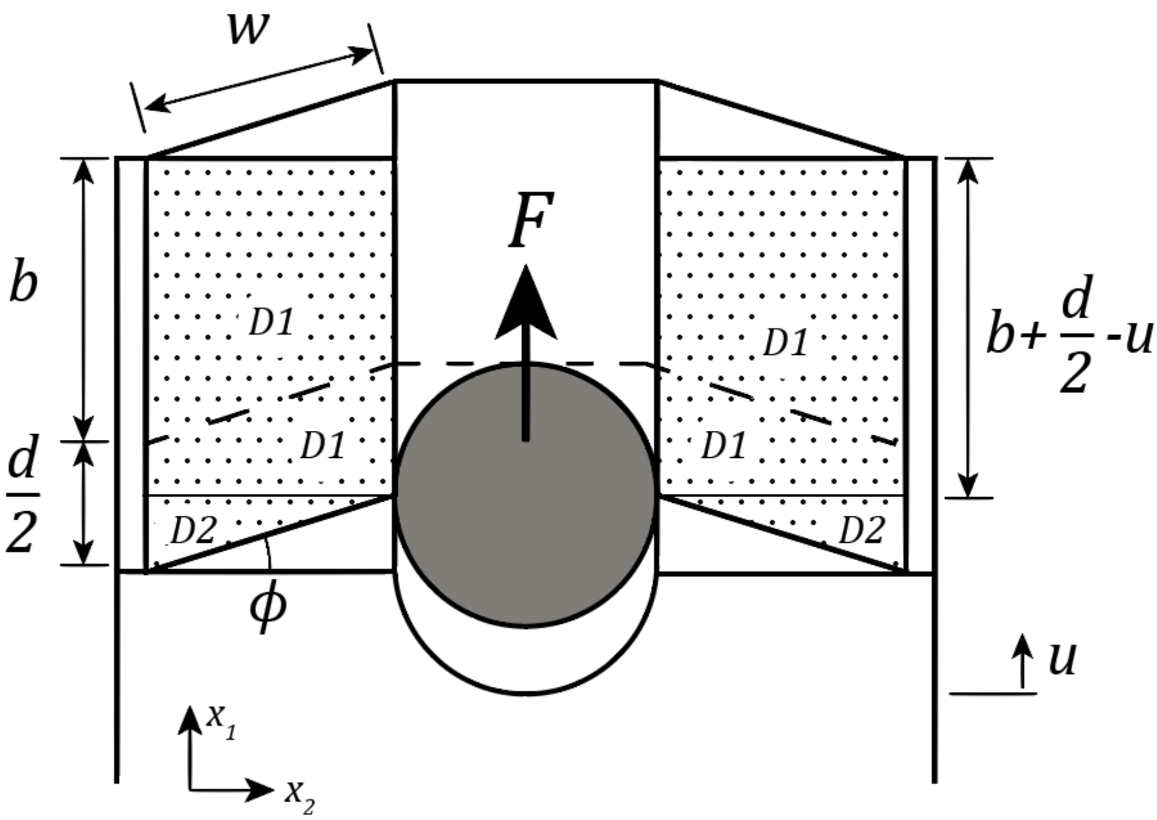

Fig. 8. Sketch of the geometry for analytical model.